Electrodynamic dust shield for surface exploration activities on the moon and Mars

C.I. Calle[1], C.D. Immer[2], J.S. Clements[3], A. Chen[4], C.R. Buhler[2], P. Lundeen[3], J.G. Mantovani[1], J.W. Starnes[2], M. Michalenko[1], and M.K. Mazumder[5]

[1]Electrostatics and Surface Physics Laboratory, NASA Kennedy Space Center, FL 32899
[2]ASRC Aerospace, Kennedy Space Center, FL 32899
[3]Physics Department, Appalachian State University, Boone, NC 28608
[4]Physics Department, Oklahoma Baptist University, Shawnee, OK 74804
[5]Department of Applied Science, University of Arkansas, Little Rock, AR 72204

Abstract

The Apollo missions to the moon showed that lunar dust can hamper astronaut surface activities due to its ability to cling to most surfaces. NASA's Mars exploration landers and rovers have also shown that the problem is equally hard if not harder on Mars. In this paper, we report on our efforts to develop and electrodynamic dust shield to prevent the accumulation of dust on surfaces and to remove dust already adhering to those surfaces.

The parent technology for the electrodynamic dust shield, developed in the 1970s, has been shown to lift and transport charged and uncharged particles using electrostatic and dielectrophoretic forces. This technology has never been applied for space applications on Mars or the moon due to electrostatic breakdown concerns. In this paper, we show that an appropriate design can prevent the electrostatic breakdown at the low Martian atmospheric pressures. We are also able to show that uncharged dust can be lifted and removed from surfaces under simulated Martian environmental conditions. This technology has many potential benefits for removing dust from visors, viewports and many other surfaces as well as from solar arrays. We have also been able to develop a version of the electrodynamic dust shield working under hard vacuum conditions. This version should work well on the moon.

Introduction

The unmanned missions to Mars and human landings on the Moon have demonstrated that dust hazards pose a pronounced threat to the future of human space exploration. Two NASA-sponsored workshops on dust mitigation conducted in 2005 concluded that developing efficient dust mitigation solutions are necessary to (1) protect all critical mission equipment, including solar panels, instrumentation and camera ports, optical mirrors, and robotic arms, against dust accumulations, (2) minimize the risk to life posed by inhalation and ingestion of toxic dusts that may contaminate air and water inside the crew cabin, and (3) reduce the contamination of extravehicular activity (EVA) suits that will otherwise become covered and severely hindered or inoperable from the constant exposure to dusts.

The development high efficiency solar panels and the urgent need of renewable energy sources on earth are likely to drive increased application of these panels in areas where sunshine is abundant throughout the year and the harvested energy is transportable to users. One such possible areas of application will be the installation of inexpensive solar panels along the highways and connecting the power output to the energy grids. Currently, national highways use solar power as a portable energy source. For low-

maintenance operation of these panels will require protection from the deposition of road dust particularly in semi-arid areas such as the sate of Arizona. In many places, natural cleaning of these panels by rains may be too infrequent and the energy conversion efficiency may decrease due to excessive deposition of dust on the surface of the panels. Laboratory experiments show that only one milligram (1.0 mg/cm^2) of dust deposited per square centimeter (1.0 mg/cm^2) may decrease the power output by more than 90 percent.

Development of a transparent, flexible electrodynamic screen (EDS) is reported here for its application to prevent any significant obscuration of the solar panels. Laboratory experiments are conducted utilizing JSC Mars-1 dust simulant and evaluations are performed under the laboratory environmental conditions at one atmosphere for terrestrial applications and at low pressures with an objective to simulate the ambient atmosphere of Mars. The following analysis show how the screen serves effectively for removing dust particles for particles of diameter smaller than 50 μm with electrostatic charge varying from zero to their saturation surface charge levels and with different electrical resistivities from conducting to highly resistive materials. The experimental studies presented here are focused on the dust removal efficiency of the test screens as a function of the size and charge distributions of the dust particles with single-phase and three-phase sine wave excitations along with their power requirements for each dust removal operations.

Removal of Dust Particles

Majority of the particles suspended in air will have diameters smaller than 50 μm of different physical properties and chemical compositions. In our experiments we have chosen Mars dust stimulants which are primarily volcanic dusts with a composition that are most likely to be present on the surface of Mars. The simulant dust samples were obtained from Johnson Space Center (JSC) and from the Jet Propulsion Laboratory (JPL). The dust samples consist of SiO2

Figure 1 illustrates the basic principles of an electrodynamic screen. In this case, a free screen is shown without the dielectric film. The electrodes can be energized either by using a single-phase or by a three-phase ac drive signal.

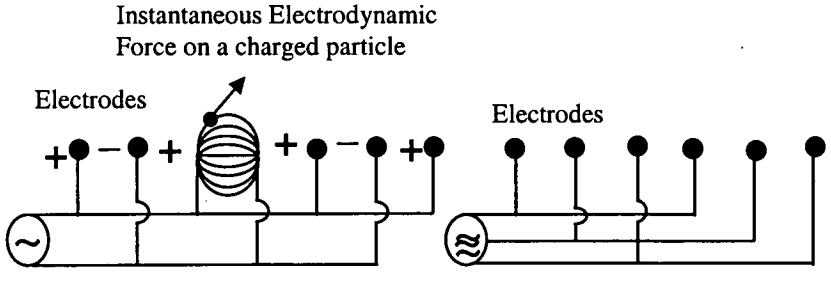

Fig. 1(left)Single-phase electric curtain. (right) Three-phase electric curtain [Masuda 1971]. The sketch shows a free screen arrangement of an electric curtain.

The single-phase excitation produces a standing wave between the electrodes and a three-phase drive that produces a traveling wave. The latter is preferable since the traveling

wave has a strong translational component that rapidly moves the dust particles from one end of the screens to the other.

The standing wave produced by single phase excitation also works well for removing the particles from the screen although not as efficiently as the three-phase. A standing wave can be considered as a superposition of two traveling waves moving in opposite directions. Thus any asymmetry or perturbation in the ac electric field, the presence of harmonies in the applied field, and any air current on the top surface of the screen produce a drift velocity to transport the levitated dust particles from the surface to move away from the screen. An example of an air current is the presence of wind on the surface of Mars.

A general equation of motion of charged particles repelled and being transported can be represented by [1-5]

$$m_p \frac{dV_p(\bar{r},t)}{dt} + 6\pi\eta r V_p(\bar{r},t) = qE_0(\bar{r})\cos\omega t + F_{ext} \qquad (1)$$

where, m_p is the particle mass, $V_p(\bar{r},t)$ is the particle velocity, η is the viscosity of the gaseous medium, r is the particle radius, q is the electrostatic charge on the particle, and $E_o(\bar{r})\cos\omega t$ is the applied electric field of angular frequency ω, and F_{ext} represents external forces, e.g. gravity. In the above equation $\bar{r}$ represents coordinates (x,y,z) whereas r is used to denote particle radius.

The electric filed E (x,y,z,t) and the resulting position of the charged particle (x, y, z, t) are related in a complex manner. Masuda, who first introduced the concept of electric curtain [2] solved the equation with approximations and his simulation agreed well with the experimental data. In the next section, we present an analytical solution of particle trajectories with simplifying assumptions. In the above equation we have assumed an initial electrostatic charge + q on the particle. However, both theoretical analysis and experimental data show that the charged and uncharged particles are both removed from the screen surface. If a particle with no initial charge (q = 0) deposit on the surface of the screen, it will soon acquire a net electrostatic charge, either by polarization of charge (dielectrophoresis) within the dielectric particle or by induction charging on a conducting particle; both processes cause a net force on the particle resulting a motion of the particle on the polymer surface. Any motion of a dielectric particle results in triboelectrification. A net charge acquired by the particles either by dielectrophoretic triboelectrification or induction causes it to be removed from the surface of the screen. Equation (1) then becomes applicable.

In most cases, particles approaching the surface of the electrodynamic screen will have a significant electrostatic charge since powder particles in the atmosphere are likely to be triboelectrically charged during their dispersion process. On the surface of Mars and on the Moon, the dust particles are likely to be highly charged. Regardless of the charging process, the total charge on individual particles is proportional to the surface area of the particle; the Coulomb force of repulsion will be

$$F_e = qE\,, \qquad (2)$$

where, $q = \sigma_s 4\pi r^2 C$, and σ_s in the surface charge density and q is the total charge in Coulombs (C). If we assume that particles are charged to their saturation level, then

$$q_s = 4\pi r^2 \times 2.64\times10^{-5} C, \quad (3)$$

where the factor $2.64\text{x}10^{-5}$ C/m^2 is taken as the maximum surface charge density of a spherical particle before an electrical breakdown at an atmospheric pressure. The maximum electric field produced on the surface of a spherical particle of charge q exceeds the breakdown voltage at the atmosphere pressure of earth (≈1000 mb) a corona discharge is initialed by the charged particle which limits the maximum surface charge density. The same process also limits the maximum charge density of the Martian dust at the ambient pressure of Mars. The maximum repulsive force at σ_s is then

$$F_{e(\max)} = q_{\max} E_{\max} = K_{\max} r^2 \quad (4)$$

where E_{max} is taken as 5 x 10^5 V/m for safe operation below the break down electric field at atmospheric pressure and K_{max} is a constant in a given ambient pressure. At the atmospheric pressure, K_{max} =112.9. The maximum limit of the electric field that can be applied on the surface of Mars is discussed later. When a particle with a saturation charge approaches the screen and is close to the surface, it will experience an electric field as shown in Fig. 1. The velocity acquired by the particle when E (t) ≈ E_{max}, can be estimated if we assume that the particles motion will obey Stokes Law. Under such assumptions, the maximum velocity of the particle in a steady state will occur when the drag resistance equals to the driving force,

$$6\pi\eta r V_p(\max) = 2.64\times10^{-5} \times 4\pi r^2 \times 5\times10^6. \quad (5)$$

For air, η = 1.8 * 10^{-5} N s/m^2, thus, the maximum velocity is proportional to the radius of the particle,

$$V_p(\max) = \frac{2.64\times10^{-5} \times 4\pi r^2 \times 5\times10^6}{6\pi\eta r}$$

$$V_p(\max) = 4.88\times10^6 \times r$$

Thus in general,

$$V_{max} = K_{max}\, r \quad (6)$$

For example, when r = 1μm, V_{max} ≈ 500 cm/s and when r = 100μm, V_{max} ≈ 50m/s.

A charged particle will acquire its steady state velocity within a time period of approximately $3\tau_p$, where τ_p is the aerodynamic relaxation time of the particle. At the atmospheric pressure on earth, τ_p = 13μs for r = 1μm, and τ_p = 30 ms for r = 50μm. For a 50μm aerodynamic diameter of a particle the value of $3\tau_p$ is 90 ms. The time period (T) of electrodynamic excitation applied to the EDS electrodes is determined from the range of values of $3\tau_p$ for the particles to be removed.

An arrangement for placing the EDS over the solar panel is shown in Fig. 2. Here the screen is composed of parallel transparent conducting electrodes embedded on the top surface of a transparent dielectric film placed over the solar panels for dust cleaning. The

screens can be placed directly over the solar panel or at a short distance over the surface covering the panel. If the electrodes are embedded within a thin dielectric film, the film serves both as a physical protection against mechanical impaction and abrasion by the dust particles particularly during a dust storm and as an electrodynamic dust shield for minimizing obscuration of incident optical radiation. The dielectric film also serves as a means to charge the uncharged particles and thus making the screen effective against both charged and uncharged dust.

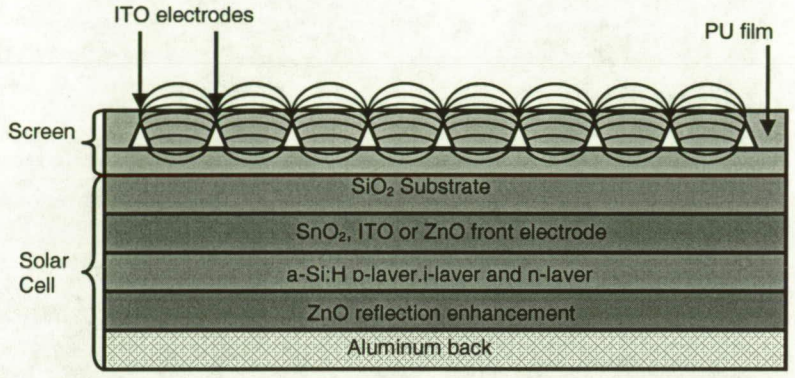

Fig. 2. Transparent electrodynamic screen embedded in a transparent film is placed over a solar panel. The Indium-Tin-Oxide (ITO) electrodes are of triangular cross-section which provides a more uniform distribution of electric field than with the electrodes of rectangular cross section.

Trajectories of Charged Particles in Electrodynamic Screen Applications

A simplified model of the positions and trajectories of drift dominated charged particles driven by traveling or standing wave voltages over electrodynamic screen is presented here. The analysis neglects the effects of particle inertia and assumes that the self-field from the particles is much smaller than the imposed field from the traveling or standing wave voltages. The traveling wave is generated by applying a three-phase electrode system embedded on the screen whereas a standing wave is formed when a single-phase electrode system is used (Fig. 1). Representative results are presented for various particle initial positions and frequencies of the applied voltage.

Traveling Wave Electric Curtain

Electric Field Solutions

Figure 3 shows the two dimensional geometry of a traveling wave potential at $x = -d$

$$v(x = -d, z, t) = V_0 \cos(\omega t - kz) \tag{7}$$

covered by a lossy dielectric layer of thickness d, permittivity ε, and conductivity σ. The region for $x > 0$ is taken to be free space with permittivity ε_0. The system is assumed to be of infinite extent in the y direction with no field dependence on the y coordinate.

In the absence of significant volume charge in the two regions $-d < x < 0$ and $x > 0$, the governing equation is Laplace's equation in both regions, $\nabla^2\Phi(x,z,t) = 0$. The necessary boundary conditions are

$$\Phi(x=-d,z,t) = v(x=-d,z,t) = V_0\cos(\omega t - kz)$$

$$\Phi(x=0_+,z,t) = \Phi(x=0_-,z,t)$$

$$\varepsilon_0\frac{\partial E_x(x=0_+,z,t)}{\partial t} = \varepsilon\frac{\partial E_x(x=0_-,z,t)}{\partial t} + \sigma E_x(x=0_-,z,t) \tag{8}$$

It is convenient to introduce complex amplitude notation so that the scalar electric potential can be written as

$$\Phi(x,z,t) = \mathrm{Re}\left[\hat{\Phi}(x)e^{j(\omega t-kz)}\right] \tag{9}$$

The solution is then

$$\hat{\Phi}(x) = \begin{cases} \dfrac{-V_0\sinh kx}{\sinh kd} + \dfrac{\hat{V}_1\sinh k(x+d)}{\sinh kd} & -d \le x \le 0 \\ \hat{V}_1 e^{-kx} & x \ge 0 \end{cases} \tag{10}$$

where $\hat{V}_1$ is the complex amplitude potential at $x = 0$

$$\hat{V}_1 = \frac{(\sigma + j\omega\varepsilon)V_0}{\sinh kd\left[j\omega\varepsilon_0 + (j\omega\varepsilon+\sigma)\coth kd\right]} \tag{11}$$

The magnitude and phase of $\hat{V}_1 = V_1 e^{-j\beta}$ are

$$V_1 = V_0\left[\frac{2(\varepsilon^2\omega^2+\sigma^2)}{(\varepsilon^2-\varepsilon_0^2)\omega^2+\sigma^2+\left((\varepsilon^2+\varepsilon_0^2)\omega^2+\sigma^2\right)\cosh 2kd + 2\varepsilon\varepsilon_0\omega^2\sinh 2kd}\right]^{1/2} \tag{12}$$

$$\beta = \tan^{-1}\left[\frac{\omega\varepsilon_0\sigma\sinh kd}{(\omega^2\varepsilon^2+\sigma^2)\cosh kd + \varepsilon\varepsilon_0\omega^2\sinh kd}\right] \tag{13}$$

Note that if $\sigma = 0$

$$V_1 = \frac{\varepsilon V_0}{\left[\varepsilon\cosh kd + \varepsilon_0\sinh kd\right]}, \quad \beta = 0 \tag{14}$$

The complex amplitude electric field in each region is then

$$\hat{E}_x = -\frac{d\hat{\Phi}}{dx} = \begin{cases} \dfrac{k\left[V_0\cosh kx - \hat{V}_1\cosh k(x+d)\right]}{\sinh kd} & -d \le x \le 0 \\ k\hat{V}_1 e^{-kx} & x \ge 0 \end{cases}$$

$$\hat{E}_z = jk\hat{\Phi} \tag{15}$$

Thus, the electric field for $x > 0$ is then

$$\begin{aligned}\bar{E} &= \mathrm{Re}\left[(\hat{E}_x \bar{i}_x + \hat{E}_z \bar{i}_z) e^{j(\omega t - kz)}\right] \\ &= kV_1\left[\cos(\omega t - kz - \beta)\bar{i}_x - \sin(\omega t - kz - \beta)\bar{i}_z\right] e^{-kx}\end{aligned} \tag{16}$$

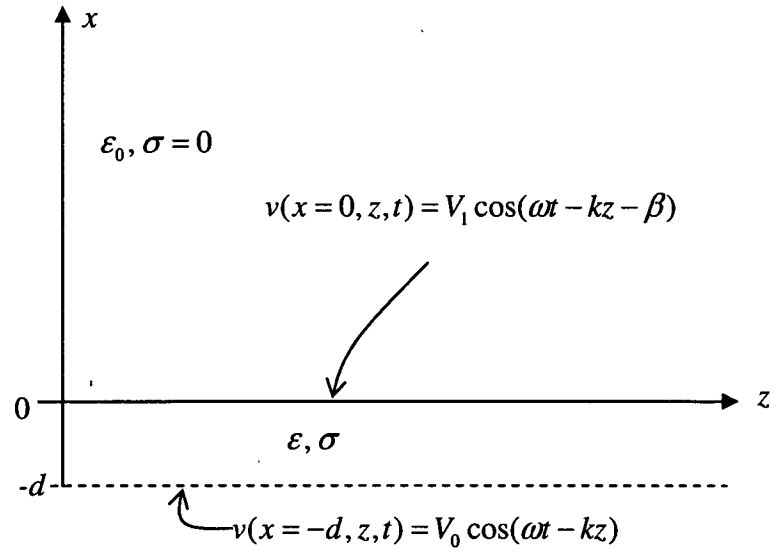

Fig. 3. A traveling wave of potential is applied at $x = -d$. A lossy dielectric layer of thickness *d*, permittivity ε, and conductivity σ prevents charged dust from penetrating into the region $x < 0$. The $x = 0$ surface has reduced potential magnitude $(V_1 < V_0)$ and a lagging phase β to the driving $x = -d$ potential.

Charged Particle Trajectories for $x > 0$

We now assume that charged particles, each with total charge ε and radius *R*, are initially uniformly distributed for $x > 0$ and that their self-field is very small compared to the field of (16). We also assume that the Coulomb force on the particles gives them a drift velocity opposed by Stokes' viscous drag where the medium for $x > 0$ has viscosity η

$$6\pi\eta R\bar{v} = q\bar{E} \tag{17}$$

The particle's mobility is then

$$\mu = \bar{v} / \bar{E} = \frac{q}{6\pi\eta R} \tag{18}$$

Neglecting particle inertia gives the *x* and *z* components of particle motion as

$$v_x = \frac{dx}{dt} = \mu E_x = \mu k V_1 \cos(\omega t - kz - \beta) e^{-kx} \tag{19}$$

$$v_z = \frac{dx}{dt} = \mu E_z = -\mu k V_1 \sin(\omega t - kz - \beta) e^{-kx} \tag{20}$$

We define a new variable

$$ku = \omega t - kz - \beta \Rightarrow \frac{du}{dt} = \frac{\omega}{k} - \frac{dz}{dt} \tag{21}$$

so that (19) and (20) can be rewritten as

$$\frac{du}{dt} = \frac{\omega}{k} + \mu k V_1 \sin ku \, e^{-kx} \tag{22}$$

$$\frac{dx}{dt} = \mu k V_1 \cos ku \, e^{-kx} \tag{23}$$

It is convenient to non-dimensionalize (21)-(23) by defining non-dimensional variables

$$\tilde{x} = kx, \ \tilde{z} = kz, \ \tilde{u} = ku = \omega t - kz - \beta, \ \tilde{\omega} = \frac{\omega}{\mu k^2 V_1}, \ \tilde{t} = k^2 \mu V_1 t \tag{24}$$

to yield

$$\frac{d\tilde{x}}{d\tilde{t}} = \cos \tilde{u} e^{-\tilde{x}} \tag{25}$$

$$\frac{d\tilde{u}}{d\tilde{t}} = \tilde{\omega} + \sin \tilde{u} \, e^{-\tilde{x}} \tag{26}$$

Taking the ratio of (25) and (26) yields an ordinary differential equation explicitly not dependent on $\tilde{t}$

$$\frac{d\tilde{u}}{d\tilde{t}} = \frac{\tilde{\omega} + \sin \tilde{u} \, e^{-\tilde{x}}}{\cos \tilde{u} \, e^{-\tilde{x}}} \tag{27}$$

which can be integrated to

$$\sin \tilde{u} = \left[\tilde{\omega}(\tilde{x} - \tilde{x}_0) + \sin \tilde{u}_0 e^{-\tilde{x}_0} \right] e^{\tilde{x}} \tag{28}$$

where the coordinate (x_0, u_0) is a point which a given charge trajectory passes through.

TABLE 1: CRITICAL POINTS $\tilde{x}_c$ AT $\tilde{u}_c = 3\pi/2$ AND MAXIMUM POSITION POINTS $\tilde{x}_m$ AT $\tilde{u} = \pi/2$ FOR VARIOUS VALUES OF $\tilde{\omega}$, $0 < \tilde{\omega} < 1$.

$\tilde{\omega}$	$\tilde{x}_c$	$\tilde{x}_m$
1	0	1.27846
0.9	0.10536	1.38383
0.8	0.22314	1.50161
0.7	0.35667	1.63514
0.6	0.51083	1.78290
0.5	0.69315	1.97161
0.4	0.91629	2.19476
0.3	1.20397	2.48244
0.2	1.60944	2.88790
0.1	2.30259	3.58105
0.01	4.60517	5.88363
0.001	6.90776	8.18622

Critical Points

Critical trajectories separate different regimes of particle motions. These critical trajectories pass through critical points where $d\tilde{x}/d\tilde{t} = 0$ and $d\tilde{u}/d\tilde{t} = 0$. Solving (25) and (26) for these zero velocity conditions gives solutions as

$$\tilde{u}_c = \frac{3\pi}{2}; \quad \tilde{x}_c = -\ln\tilde{\omega} \tag{29}$$

where without loss of generality we only consider $\tilde{\omega} > 0$. Note that since $\tilde{x} > 0$, critical points can only occur if $0 < \tilde{\omega} < 1$.

Table 1 lists some values of $\tilde{x}_c$ and also the maximum position $\tilde{x}_m$ at $\tilde{u} = \pi/2$ that charge can travel from $\tilde{x}_0 = 0$ through the critical point $\tilde{x}_c$. Note that the values of $\tilde{x}_c$ and $\tilde{x}_m$ increase as $\tilde{\omega}$ decreases.

Charge initially outside the critical trajectory cannot reach the $\tilde{x} = 0$ surface. Charge initially on the $\tilde{x} = 0$ surface travels synchronously with the voltage traveling wave, within an envelope of the charge trajectory that passes through the critical point $(\tilde{x} = \tilde{x}_c, \tilde{u} = 3\pi/2)$.

Standing Wave Electric Curtain

Electric Field Solutions

We now replace the traveling wave voltage at $x=0$ in Figure 3 by a standing wave

$$v(x=-d,z,t)=V_0\cos\omega t\cos kz \tag{30}$$

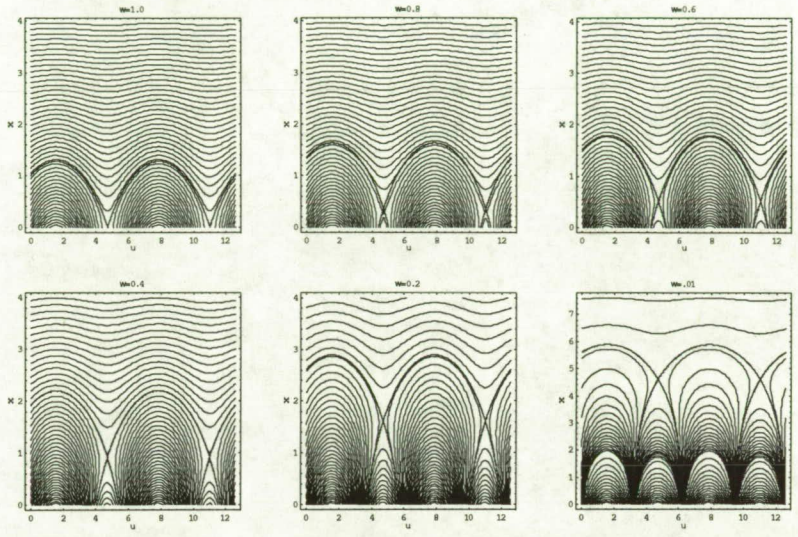

Fig. 4. Non-dimensional charge trajectories in $(\tilde{x},\tilde{u})$ space for various values of $\tilde{\omega}$, for $0<\tilde{\omega}\le 1$, for a traveling wave voltage given by (7). Note the critical separation trajectories passing through the point $(\tilde{x}=\tilde{x}_c,\tilde{u}=3\pi/2)$ that separates charged particle regions. The maximum position of charge that travels from $\tilde{x}=0$ occurs at $(\tilde{x}=\tilde{x}_m,\tilde{u}=\pi/2)$. The values of $\tilde{x}_c$ and $\tilde{x}_m$ for various $\tilde{\omega}$ are listed in Table 1.

Then, the solution for the scalar electric potential is of the form

$$\Phi(x,z,t)=\mathrm{Re}\left[\hat{\Phi}(x)\cos kz\, e^{j\omega t}\right] \tag{31}$$

where $\hat{\Phi}(x)$ is of the same form as (10). The boundary conditions are still given by (8) with the traveling wave potential at $x=-d$ replaced by (30). Then the solutions of (11)-(14) are valid here and the electric field for $x>0$ is

$$\overline{E}=kV_1\cos(\omega t-\beta)\left[\cos kz\,\overline{i}_x+\sin kz\,\overline{i}_z\right]e^{-kx} \tag{32}$$

Charged Particle Trajectories

The analogous charge transport equations to (19) and (20) are

$$v_x=\frac{dx}{dt}=\mu E_x=\mu kV_1\cos(\omega t-\beta)\cos kz\, e^{-kx} \tag{33}$$

$$v_z=\frac{dz}{dt}=\mu E_z=\mu kV_1\cos(\omega t-\beta)\sin kz\, e^{-kx} \tag{34}$$

Introducing the non-dimensional variables

$$\tilde{t} = \omega t - \beta, \quad \tilde{x} = kx, \quad \tilde{z} = kz, \quad \tilde{\omega} = \frac{\omega}{\mu V_1 k^2} \tag{35}$$

reduces (33) and (34) to

$$\frac{d\tilde{x}}{d\tilde{t}} = \frac{\cos\tilde{t}\cos\tilde{z}\, e^{-\tilde{x}}}{\tilde{\omega}} \tag{36}$$

$$\frac{d\tilde{z}}{d\tilde{t}} = \frac{\cos\tilde{t}\sin\tilde{z}\, e^{-\tilde{x}}}{\tilde{\omega}} \tag{37}$$

To solve (36) and (37) we relate them through the common factor

$$\frac{\cos\tilde{t}\, e^{-\tilde{x}}}{\tilde{\omega}} = \frac{1}{\cos\tilde{z}}\frac{d\tilde{x}}{d\tilde{t}} = \frac{1}{\sin\tilde{z}}\frac{d\tilde{z}}{d\tilde{t}} \tag{38}$$

Eliminating the $d\tilde{t}$ yields

$$\frac{d\tilde{x}}{d\tilde{z}} = \cot\tilde{z} \tag{39}$$

with solution

$$\sin\tilde{z}\, e^{-\tilde{x}} = \sin\tilde{z}_0\, e^{-\tilde{x}_0} \tag{40}$$

where $\tilde{x}_0$ and $\tilde{z}_0$ are initial coordinates of a particle at $\tilde{t} = 0$.

The substituting (40) into (37)

$$\frac{d\tilde{z}}{d\tilde{t}} = \frac{\cos\tilde{t}}{\tilde{\omega}}\sin\tilde{z}_0\, e^{-\tilde{x}_0} \tag{41}$$

allows solution for $\tilde{z}(\tilde{t})$

$$\tilde{z}(\tilde{t}) = \frac{\sin\tilde{t}\sin\tilde{z}_0\, e^{-\tilde{x}_0}}{\tilde{\omega}} + \tilde{z}_0 \tag{42}$$

with $\tilde{x}(\tilde{t})$ obtained from (34) as

$$\tilde{x}(\tilde{t}) = \ln\left[\frac{\sin\tilde{z}(\tilde{t})}{\sin\tilde{z}_0}\right] + \tilde{x}_0; \quad \tilde{x}_0, \tilde{x}(\tilde{t}) \geq 0 \tag{43}$$

Representative charge particle trajectories in $(\tilde{x}, \tilde{z})$ space for various frequencies $\tilde{\omega}$ are shown in Figure 5. While (40) shows that $\tilde{z}(\tilde{t})$ varies purely sinusoidally with time, (43) shows $\tilde{x}(\tilde{t})$ has a non-linear variation with time.

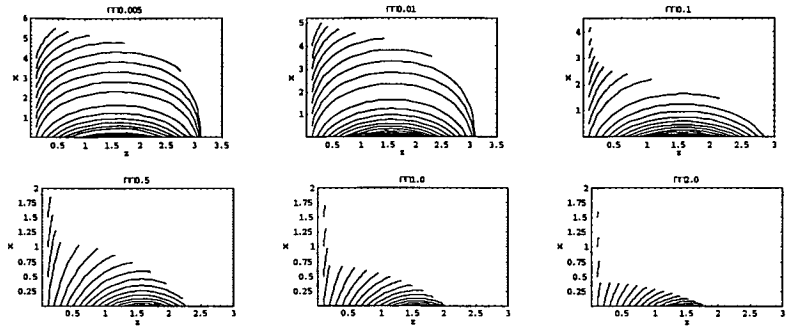

Figure 5. Non-dimensional charge trajectories in $(\tilde{x}, \tilde{z})$ space for various values of $\tilde{\omega}$ with a standing wave voltage given by (24).

The above analysis shows that the electrodynamic screen, driven either by a single-phase or a three-phase ac sine wave, acts as a screen that does not allow charged particles to penetrate the electrical field barrier and deposit on the plane x = 0.

Removal of uncharged particles

When the electrodes are embedded within a dielectric film, and are excited with sine waves as shown in Figs. 6, 7, 8, and 9, it has been experimentally observed that both initially charged and uncharged particles with different electrical resistivities are efficiently removed from the electrodynamic screen. The removal process for an initially charged (q) particle as shown in Fig. 6, has been discussed in the previous section and for uncharged dielectric particles, the process is illustrated in Fig. 7 and 8. Figure 9 shows the induction charging of an uncharged conducting particle on the electrodynamic screen.

By virtue of the dipole moment induced on the particle place in a non-uniform electric field, the particle experiences dielectrophoretic force in the field gradient [6],

$$F_d = (\overline{P}\nabla)\vec{E}, \tag{44}$$

where, $\overline{P}$ is the polarization vector and is equal to np, where p = qd, the dipole moment for each individual dipoles within a single particle and n is the number of the dipoles. For a spherical particles of radius r, and of dielectric constant ε_2 exposed to a field gradient as expressed in (44), while being placed on a film of dielectric constant ε_1, the force can be represented as [7]

$$\vec{F}_d = 2\pi r^3 \varepsilon_1 \frac{\varepsilon_2 - \varepsilon_1}{\varepsilon_2 + \varepsilon_1} \nabla |E|^2 \tag{45}$$

The direction of the field depends upon the sign of the term $(\varepsilon_2 - \varepsilon_1)$. The dielectric constants of the particle and that of the film are assumed loss-less.

The waveform of an applied voltage $V_o \sin(\omega t)$ in a single phase operation is represented in figures 6-9. Figure 5 represents the dust removal process when a charged particle arrives close to the screen surface. If q = 0, the particle will settle on the screen surface. Once the particle is on the surface as shown in Fig. 6, the particle will acquire a charge as explained above.

Since the applied divergent electric field oscillates, the particle experiences a periodic force whose magnitude is proportional to the square of the field intensity. The fluctuations of the force of attraction on the particle make it to roll or move along the field gradient lines on the dielectric surface. These particle motions on the polymer surface produces triboelectrification as discussed above, to a significantly high charge level as the particle charge continues to increase as the particle motion increases as it gains additional charge. The resulting net charge on the particle causes the particles to jump off of the screen. Figs. 7 and 8 illustrate the particle motion.

The excitation voltage waveform,Vo sin ωt, the electric field $E_o\cos(\omega t)$, and the resultant velocity of a tribocharged particle (assumed as +q), will result in a particle motion $V_p(t) = V_{po}\cos(\omega t - \phi)$ as shown in Fig. 7. The charged particle undergoes an oscillation along the curved lines of force between the adjacent electrodes. The figure shows a positively charged particle is experiencing two forces of repulsion, one tangential to the curved field lines and the other normal to the curved path. The normal component is the centrifugal force arises due to the curvilinear inertial motion of the particles. This normal component provides the lift force normal to the surface of the screen.

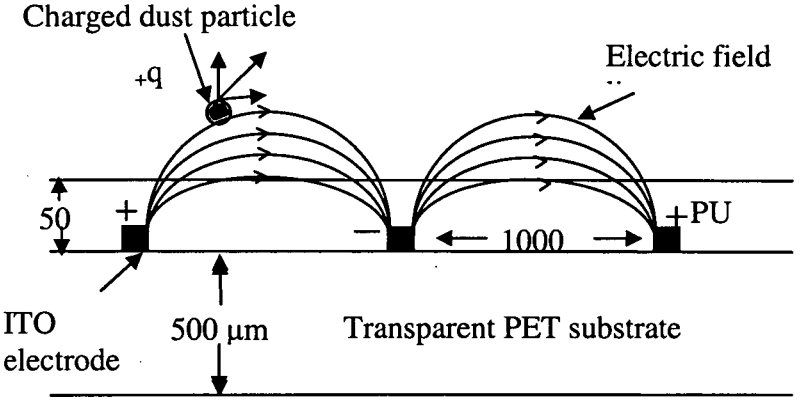

Fig.6. Cross section of an Electro-dynamic Screen made of a flexible polyethylene terephthalate (PET) film of 500 μm thickness on which transparent Indium Tin Oxide (ITO) electrodes of rectangular cross section (width 10μm, height 10μm) are deposited with an inter-electrode spacing of 1000□m. The electrodes are embedded within a polyurethane (PU) film coating with a film thickness of 50 μm. The thickness of the electrodes is varied from 10 to 100 μm and the interelectrode spacing from 100 μm to 1000 μm for optimization of EDS operation.

As the particles oscillate or roll initially with a small amplitude due only to the dielectrophoretic force, then with increasing amplitudes as contact charging continues due to the associated friction against the surface of the screen, the particle charge increases, the polarity and magnitude of the charge depends upon the work function difference between the two contacting surfaces charged by the induction charging process. The process is similar to the charging of the dielectric particles. In general, particle charging takes place by all of these mechanisms combined with contributions at different degrees depending upon the materials involved. Table 2 shows the relative contributions.

Uncharged conducting sphere

The process of electrostatic charging and removal also works for conducting particles. The particles, initially uncharged and deposited on the dielectric screen, will experience a force due to the induced charge. The charge on a spherical particle can be approximated as [6] $q \propto E_0 r^2$.

The above analysis is applicable to inorganic dust particles that are not highly adhesive on the screen surface. In general, the induction force can be represented by

$$F_i \propto E_0^{\,2} r^2 \tag{47}$$

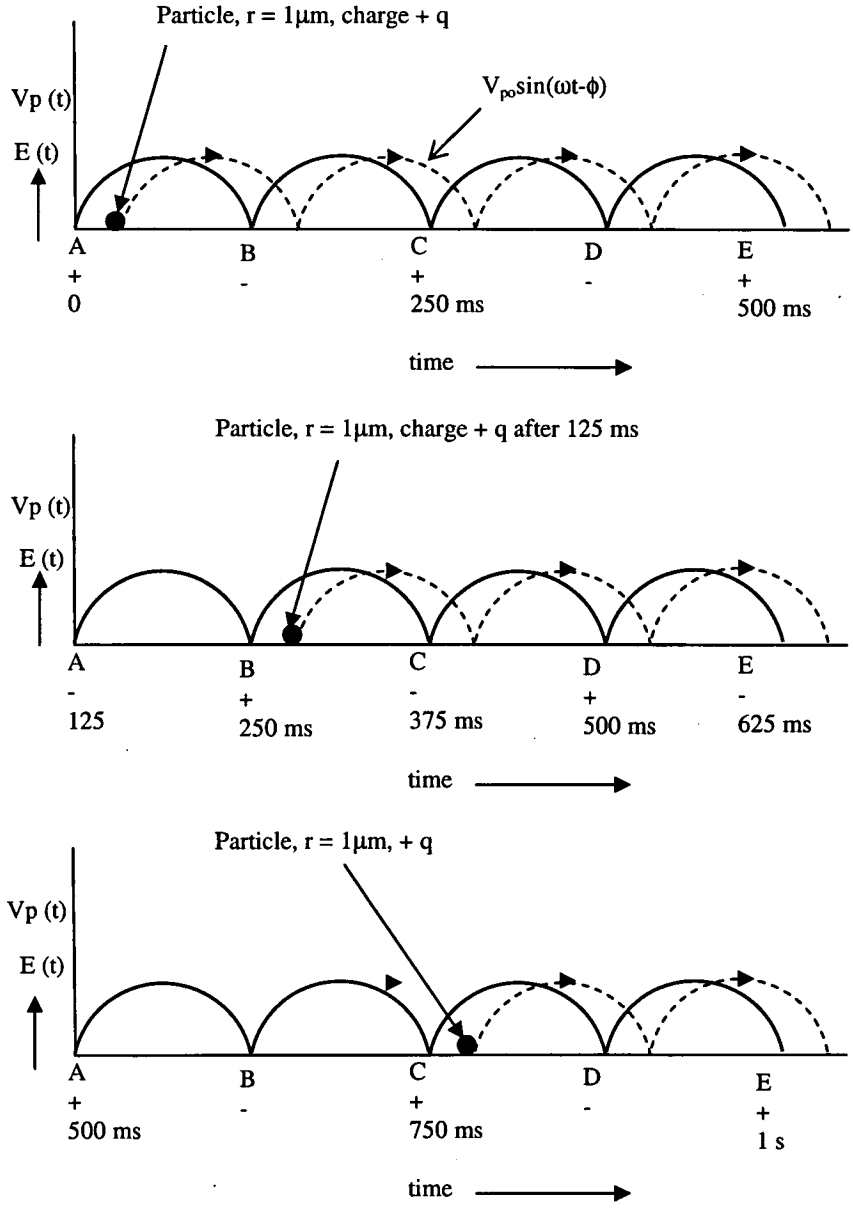

Fig. 7. A charged (+q) particle of diameter 2 mm – located at A is subjected to an AC electrical field E_o sin ωt applied between the adjacent electrodes as shown. We assume the position of the particle as a function of time is shown in three time frames, starting at t_1=0 (top frame), t_2=125 ms

(middle frame), and at t_3 = 500 ms (bottom frame) respectively. The steady state particle velocity is represented by $V_{po}\sin(\omega t-\phi)$ where ϕ is the phase lag for the particle, given by $\tan^{-1}\omega\tau_p$, where τ_p is the aerodynamic relaxation time.

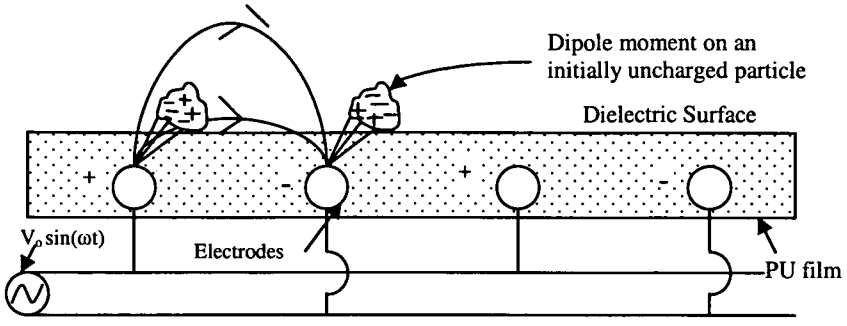

Fig. 8 An uncharged dielectric particle deposited on the surface of the dielectric film is experiencing a dielectrophoretic force because of the induced dipole moment on the particle by the applied electric field. Since the applied electric field oscillates, the particle experiences a force proportional to the square of the field gradient and moves along the field lines on the dielectric surface and is tribo-electrified to a significantly high charge. Thus the initially uncharged particles are polarized and experience a dielectrophorehic force that produces a net charge on the particle which causes additional tribo-electrification until the particles jump off of the screen.

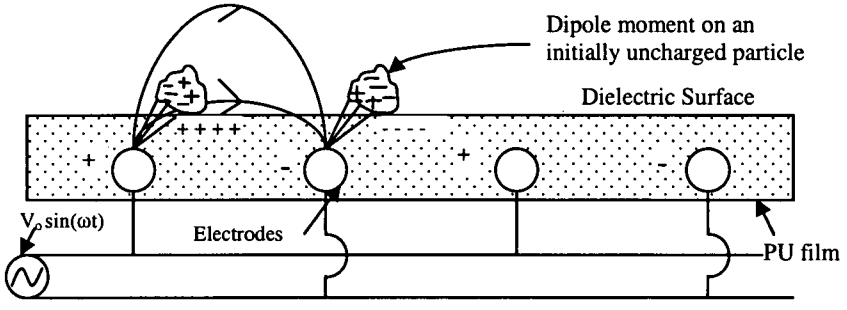

Fig. 9 Induction charging of conducting and semi-conducting particles deposited on a dielectric screen with embedded electrodes ε_1 and ε_2 are the relative dielectric constants of the screen and the particle respectively.

The induction charging time constant of a particle resting on a dielectric screen will depends upon the conduction of the charge that has the same polarity as the instantaneous polarity of the electrode from the particle to the dielectric surface of the screen. In many applications of the EDS, it is assumed that the particles are of lossy dielectric materials and the screens will also have a significant surface conductivity for charge conduction from the particles. It is necessary to have a limited amount of surface conductivity to avoid charge accumulation on the surface of the dielectric screen.

TABLE 2. ELECTROSTATIC CHARGING PROCESSES FOR INITIALLY UNCHARGED PARTICLES DEPOSITED ON AN ELECTRODYNAMIC SCREEN EMBEDDED IN AN INSULATIVE POLYMER FILM.

Particle Resistivity	Charging Processes	Limitations
$\rho < 10^8\ \Omega m$	Induction and Triboelectrification	Film surface resistivity too high; High Humidity; R< 0.5 μm; & Low Electric Field.
$10^8\ \Omega m < \rho < 10^{11}\ \Omega m$	Induction, Dielectrophoretic motion, and Triboelectrification	Same as above
$\rho > 10^{11}\ \Omega m$	Dielectrophoretic motion and Triboelectrification	Same as above & Low work function difference between the contacting surfaces.

The induction charging time constant of a particle resting on a dielectric screen will depends upon the conduction of the charge that has the same polarity as the instantaneous polarity of the electrode from the particle to the dielectric surface of the screen. In many applications of the EDS, it is assumed that the particles are of lossy dielectric materials and the screens will also have a significant surface conductivity for charge conduction from the particles. It is necessary to have the necessary amount of surface conductivity to avoid charge accumulation on the surface of the dielectric screen.

The requirement of surface conductivity is a critical factor in the operation of EDS for all three cases of particles on the film surface. An excessive surface conductivity will shield the electric field whereas a very high resistivity will lead to an excessive accumulation of surface charge on the film that will affect the applied field, reduce tribocharging and increase particle adhesion to the surface. Since the time constant for charging of the particle will depend upon the product of resistivity (ρ_p) and the dielectric constant (ε) of the particle, the effective surface resistivity of the particle will also depend upon the surface resistivity of the screen. If ρ_p is the effective resistivity of the particle on the screen surface, then the charging time constant (τ_c) can be approximated as

$$\tau_c = \varepsilon_2 \varepsilon_0 \rho_p \tag{48}$$

$$\varepsilon_0 = 8.854 \times 10^{-12} F/m$$

Induction charging takes place for all materials but becomes effective when

$$\tau_c << T$$

where T is the time period of the applied electric field $E_0 \sin \omega t$ and ε_0 is the permittivity of free space. For example, if $\rho_p = 10^8$ Ωm, and $\varepsilon_2 = 2.0$, the charging time constant will be approximately 2 ms, which is much shorter than 250 ms time period (T) if the applied ac field has a frequency of 4 Hz. Figure 7 shows an example of a particle trajectory for a 2μm diameter particle which has acquired a positive charge q during the half cycle before t = 0+, the trajectory of the particle will be identical to the particle as shown (Fig. 7).

For particles with higher resistivity, the charging is due primarily to the combination of dielectrophoresis, induction and triboelectrification. In the application related to dust mitigation on the surface of Mars and the moon, where the ambient humidity effect is negligible, the charging process will not be affected by the moisture content.

Experimental description

Experimental Setup

1. Sample preparation: Experiments on testing the test electrodynamic screens for their Dust Removal Efficiency (DRE) were carried out with JSC Mars-1 dust simulant. The dust samples were obtained from the Jet Propulsion Laboratory, Pasadena, CA. Before each test, the sample was dried in an oven at a temperature of 100°C for at least 24 hours. For each experimental run, a small amount of dust was dispersed using a powder pump, a venture suction device for aerodynamic dispersion of dust in air forming an aerosol. Alternatively, a blow-off cup [8] was used for tribocharging and dispersion of dust.

2. Size classification: The aerosols containing dust particles were classified by using a cyclone classifier that removed the coarse particles, with diameter larger than 10 μm. The fine fraction of aerosol used for test had particles whose Count Median Diameter (CMD) ranged from 2 to 6 μm, and Voulme (or Mass) Median diameter (MMD) ranging from 8 to 15 mm. This size range agrees with the anticipated Martian dust cloud, as shown in Table 3 (operational condition of the electrodynamic screen).

3. Charging and Charge Neutralization of Dust Cloud: For charging the particles of test aerosol, corona chargers were used for unipolar charging, either with positive or negative polarity. In most cases however, the dust particles were tribocharged by tumbling against Stainless Steel or Teflon beads in a Stainless Steel or Teflon® lined containers. These processes were reported earlier [8, 11, 12]. The dust cloud generated, irrespective of their dispersion process contained charged particles. For neutralizing the dust particles, a charge neutralizer (Simco Model PFC 20) was used. Charge neutralization was necessary to test screen against uncharged particles.

4. Electrodynamic Screen: The electrodynamic screens (EDS) were fabricated as printed circuit boards. The screens were coated with polyurethane prior to use to prevent electrical arcing at high voltages. The screens were tested at a several operational parameters (frequency, voltage, run time) for optimum performance. EDS were tested for uncharged, charged and neutralized dust particles.

5. Test Procedure: A dust cloud chamber, with appropriate ventilation was used for testing the EDS devices operating then either with single- or three-phase ac drive. The test EDS was placed near bottom of the chamber while the test aerosol was introduced at the top. The size and charge distribution of particles was measured using ESPART analyzer. The size distribution of the simulant dust was also measured using Microtrac® analyzer. The dust removal efficiency (DRE) of EDS was calculated by measuring the total mass of dust on screen before and after it was energized.

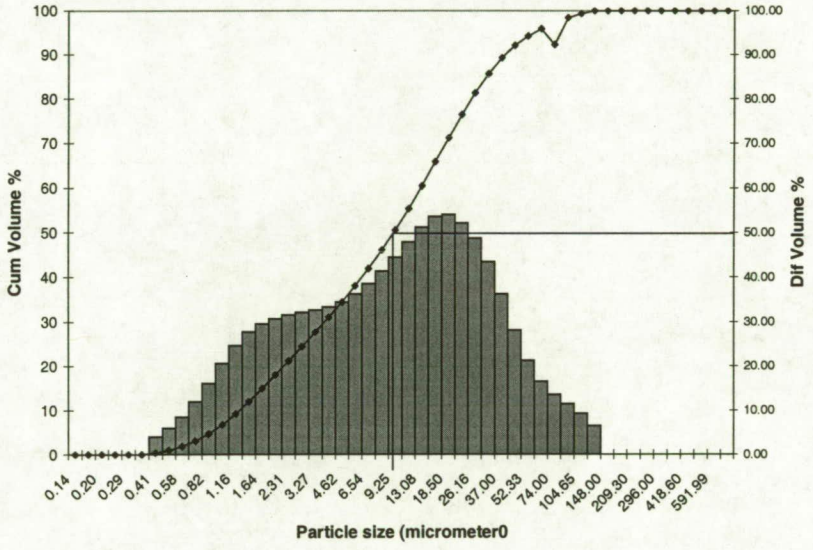

Fig.10. Particle size distribution of JSC Mars-1dust simulant using Microtrac® analyzer

Results

The particle size analysis of JSC Mars-1 simulant dust using Microtrac® analyzer is shown in Fig. 10. The d_{10}, d_{50}, d_{90} was found to be 1.22 μm, 9.06 μm and 38.45 μm respectively. The count median diameter of simulant dust using ESPART analyzer was 3.66μm (STDEV 0.19, n= 15) as shown in Fig. 11.

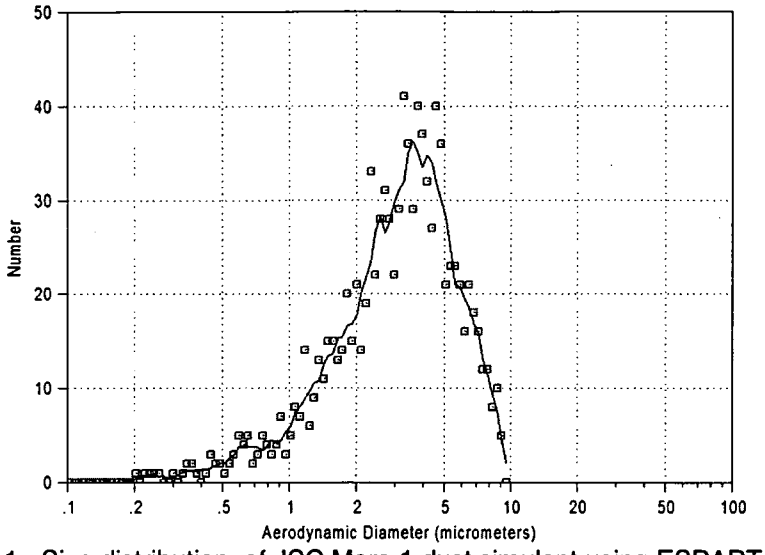

Fig. 11. Size distribution of JSC Mars-1 dust simulant using ESPART analyzer

The charge-to-mass ratio (Q/M) of simulant dust using ESPART analyzer was -2.7 μC/g (Fig. 13). This charge distribution was the result of (1) inter-particle charging, (2) tribocharging during grinding, and (3) handling processes. The simulated dust samples were not milled or corona charged

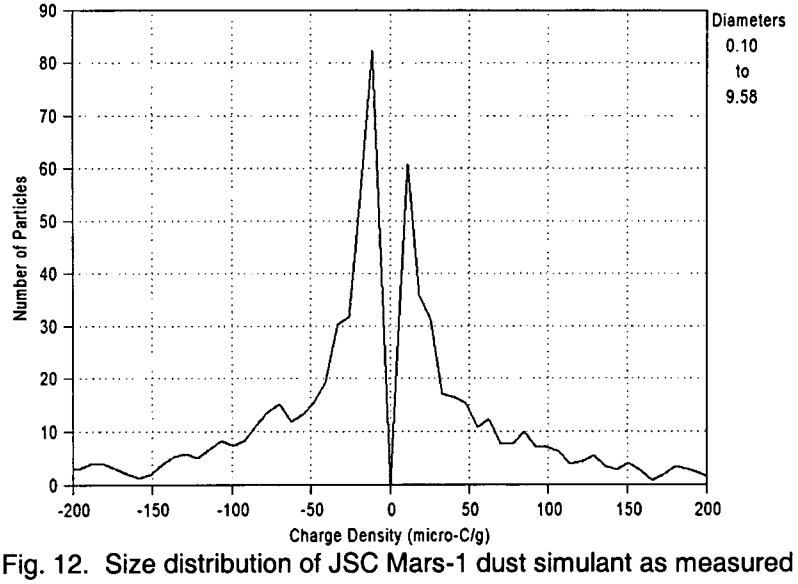

Fig. 12. Size distribution of JSC Mars-1 dust simulant as measured by ESPART analyzer

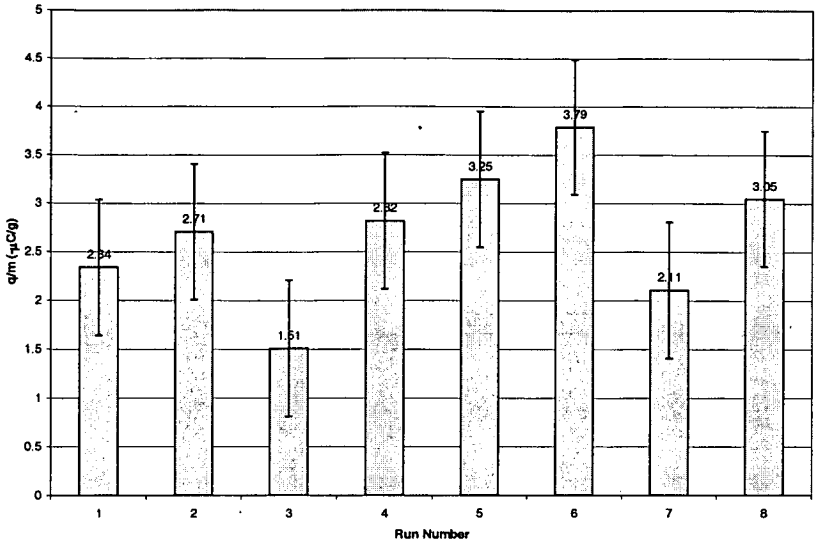

Fig. 13. Charge-to-mass ratio of JSC Mars-1dust simulant particles as measured by using an ESPART analyzer. The particles were naturally charged.

When the dust cloud particles were treated for either additional tribocharging or discharging, it was observed that the simulant dust charged positively against Teflon and negatively against stainless steel in both air and CO_2 atmosphere [11, 12]. When particles were neutralized, most of the particles showed charge close to zero. However, the Q/M for the simulant dust decreased significantly in the dry CO_2 environment. Further, the performance of screen was also analyzed for neutral particles (Figure 4). It was found that the DRE of screen did not deteriorate for neutral particles.

An effective voltage, waveform, and frequency for dust removal at the atmospheric pressure using single phase EDS systems [9-12]. A dust removal efficiency of 85% was obtained for charged JSC Mars-1 dust simulant when excited by single phase AC [9]. The effect of particle size on dust removal efficiency of three-phase EDS system showed three-phase operation is advantageous [10-12]. A dust removal efficiency of over 90% was achieved for an EDS with 1.27 mm electrode spacing (Fig. 14).

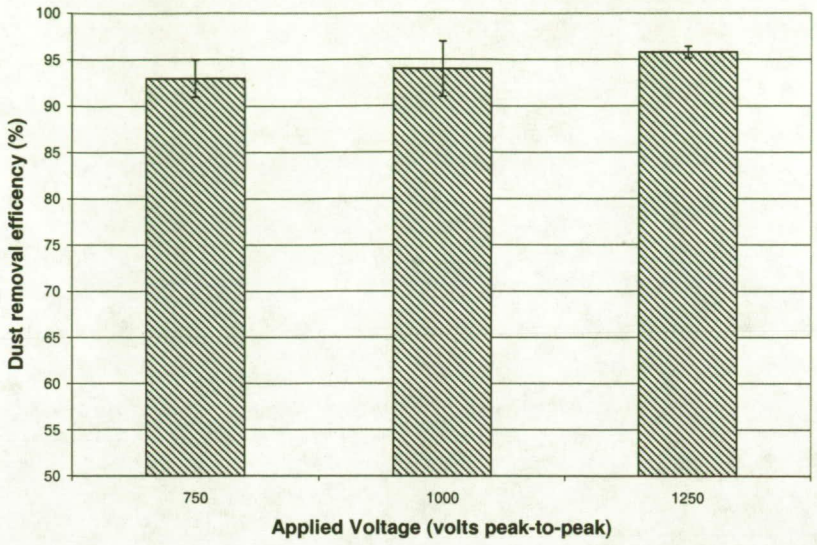

Fig. 14. Dust removal efficiency of a three-phase electrodynamic screen operating at 750, 1000 and 1250 volts (Electrode spacing 1.27mm, trace 0.127 mm, 4 Hz, cleaning operation time 30 s.

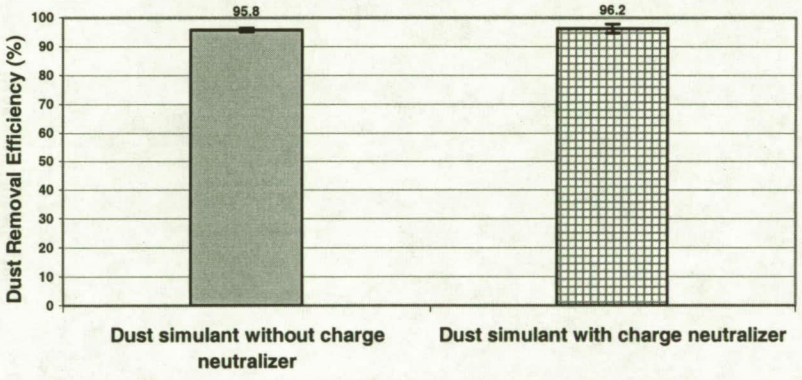

Fig. 15. Dust removal efficiency of a 3-phase electrodynamic screen with and without charge neutralizer (Electrode spacing 1.27 mm, trace 0.127mm, 1250 V peak-to-peak, 4 Hz, run time 30 s, Count Median (Aerodynamic) Diameter= 3.66 □m, d_{10}= 1.22 □m, d_{50}=9.06 □m, d_{90}=38.45 □m).

Discussion

We presented here the basic principles of electrodynamic screen operation for removing dust particles. Performance of the EDS in also presented to show the Dust Removal Efficiency (DRE) is greater than 80% for the desired size and charge range of particles anticipated in the Martian atmosphere.

The mathematical analysis provides a closed form expressions for the position of charged particles driven by traveling and standing wave voltages. Representative solutions of particle trajectories have been presented as a function of initial positions and frequency. The next phase of this work will take parameters of actual experiments and plot out the

calculated charged particle trajectories and relate them to the efficiency of the electrodynamic screen.

The analysis presented here has made simplifying assumptions that charged particle inertia is negligible and that the self-field from the charged particles, including image forces, are negligible compared to the imposed fields from the traveling and standing wave voltages. The next phase of this analysis will attempt to relax these assumptions to examine the inertial and self-field effects.

The test results also show that EDS operation remains efficient for all of the three charging conditions: (1) positively charged particles, (2) negatively charged particles, and (3) particles with a net charge close to zero. The design for constructing the EDS has also been empirically optimized. However, most of test performed to date were conducted in the atmospheric pressure and at low atmospheric pressure above 100mb.

Table 3 shows the atmospheric conditions of the Moon and Mars. Since the atmospheric pressure on mar rages from 0.75 to 7.5mb at an ambient temperature varies from –70 to 20°C. There is no atmosphere on the surface of the Moon.

TABLE 3: OPERATIONAL CONDITIONS FOR ELECTRODYNAMIC SCREENS (EDS) ON THE MOON AND MARS.

Surface Properties	Moon	Mars
Gravitational force	0.165g (1/6g)	0.38g (1/3 g)
Surface Atmospheric pressure	10^{-8} mb	0.75 to 7.5 mb
Primary Atmospheric composition	No atmosphere	95% CO_2 ; 2.7% N_2 0.15 % O_2 , 0.03% H_2O (No Liquid water)
Surface Temperature variation	varies widely -223C to 123 C (dark) (sunlight)	Average: -63C -70C to 20 C
Windspeed	strong solar wind	2 to 10 m/s; up to 30 m/s dust storm
Viscosity	No atmosphere	$1.014 * 10^{-5}$ N*s/m^2
Atmospheric dust Surface layer	No atmosphere Thick layer of surface dust coated with magnetic material	Dusty atmosphere $9 * 10^{-8}$ kg/m^3 (normal) $7 * 10^{-5}$ kg/m^3 (dust storm) PSD: 0.5 to 50 m (dia) CMD = 1 . 6 m dia Thick layer of surface dust
Magnetic Field	No global magnetic field Does not shield solar wind	Lost its magnetic field 3.5 billion years ago, but has strong local or crustal magnetic field
Global Electric Field Electrical Breakdown	Charged dust surface Paschen breakdown can occur at a low voltage ~ 100V	High localized electric field during dust devils. Paschen breakdown voltage ~ 700V

A major problem is operating the EDS will be to avoid Paschen breakdown of the electrodynamic field applied on the screen at the Martian pressure. The breakdown voltage or the sparking potential, according to Paschen's Law is a function for the product pd where p is the ambient pressure and d is the distance between the electrodes. The breakdown field is not a linear function of pd; it depends upon the actual value of d and the number of collision made by the electron in crossing the gap d which depends upon the density of gas.

We are currently optimizing the distance d and the electric field to grater EDS at an ambient pressure down to 5mb, at CO_2 atmosphere. Screens have also been developed for high vacuum conditions, simulating the lunar environment. At these extremely low pressures, Paschen's law allows very high potentials. The limitation on the potentials comes from the electrode proximity and the breakdown properties of the substrate and the coatings applied to the electrodes themselves.

Conclusions

The electrodynamic screens (EDS) are made of transparent plastics, such as PET for its UV radiation resistance, and a set of parallel conducting electrodes, made of transparent Indium Tin Oxide (ITO) or a conducting polymer, embedded under a thin transparent film on the surface. The transparent plastic film EDS can be efficiently used for protecting solar panels from dust deposition and obscuration of solar radiation. By applying a three-phase high voltage AC electric field to the electrodes, the resulting electrodynamic field repels and removes dust particles from the screens regardless of whether the dust particles are initially charged or uncharged. Test results show that self-cleaning solar panels may be manufactured incorporating electrodynamic screens that will derive its power - about one Watt per square meter of a solar panel which produces a peak output of approximately 800 Watts. Considering additional loss in the three-phase HV power supply, it is estimated that approximately 10 Watts may be needed from the solar panel, a small fraction, only when cleaning is needed. Under the normal atmospheric conditions on Mars, only a few minutes of cleaning will be needed per sol. More frequent cleaning will be needed during dust storms. The electrodynamic screens have also been shown to work at the hard vacuum conditions of the lunar environment.

Acknowledgements

Both the theoretical and experimental studies are being pursued jointly at the Department of Applied Science, University of Arkansas at Little Rock (UALR), Laboratory for Electromagnetic and Electronic Systems, Massachusetts Institute of Technology, Electrostatics and Surface Physics Laboratory, NASA Kennedy Space Center, the NASA Jet Propulsion Laboratory and Appalachian State University (ASU), NC. The research was supported by a NASA Grant NRA 02-0SS-01 (ROSS-2002), JPL Contract No. 1263202. Praveen Srirama, David Clark and Chris Wyatt of UALR for their contributions to this study.

References

[1] S. Masuda, "Electric Curtain for Confinement and Transport of Charged Particle Clouds," in *Advances in Static Electricity*, 1, Auxilia, S.A., Brussels, pp. 398-414, 1970.

[2] S. Masuda, "Electric Curtain for Confinement and Transport of Charged Aerosol Particles," *Proceedings of Albany Conference on Electrostatics*, 1971.

[3] S. Masuda, K. Fujibayashi, K. Ishida, and H. Inaba, "Confinement and transportation of charged aerosol clouds by electric curtain," *Electronic Engineering in Japan*, **92**, pp. 9-18, 1972.

[4] S. Masuda, and Y. Matsumoto, "Contact-type Electric Curtain for Electrodynamical Control of Charged Dust Particles," *Proceedings of the 2nd International on Static Electrification*, Frankfurt, 1973.

[5] J. R. Melcher, "Traveling-wave induced electroconvection," Phys. Fluids, vol. 9, no. 8, pp. 1548–1555, 1966.

[6] J. A. Cross, *Electrostatic Principles, Problems and Applications*, Bristol, U. K: Adam Hilger, 1987.

[7] H. A. Pohl, *Dielectrophoresis*, Cambridge University Press, Cambridge, 1978.

[8] S. Trigwell, "Correlation between Surface Structure and Tribocharging of Powders," *Ph.D. dissertation*, Dept. Appl. Sci., Univ. of Arkansas at Little Rock, Little Rock, AR, 2003.

[9] A. S. Biris, D. Saini, P. K. Srirama, M. K. Mazumder, R. A. Sims, C. I. Calle, C. R. Buhler, "Electrodynamic removal of contaminant particles and its applications," IEEE-IAS 39th Annual Meeting, Seattle, WA, 2004.

[10] C.E. Johnson, P.K. Srirama, R. Sharma, K. Pruessner, J. Zhang and M.K. Mazumder: Effect of Particle Size Distribution on the Performance of Electrodynamic Screening Systems, IEEE-IAS 40th Annual Meeting, Hong Kong, 2005.

[11] R. Sharma, P. K. Srirama, M. K. Mazumder, D. W. Clark, "Electrostatic Properties of Mars/ Lunar Dust Simulants and their Effects on the performance of Dust Mitigation Devices," Space Resources Roundtable VII: LEAG Conference on Lunar Exploration, League City, Texas, 2005.

[12] M. K. Mazumder, A. S. Biris, C. U. Yurteri, R. A. Sims, R. Sharma, C.E. Johnson, K. Pruessner, C.I. Calle, S. Trigwell, C.R. Buhler, and J.S. Clements, "Solar Panel Obscuration by Dust in the Martian Atmosphere," Particles on Surfaces 9: Detection, Adhesion And Removal, VSP, 2006 (In Press).